

Article

Influence of Plasma Surface Treatment of Polyimide on the Microstructure of Aluminum Thin Films

Eiichi Kondoh

Faculty of Engineering, University of Yamanashi, Kofu 400-8511, Japan; kondoh@yamanashi.ac.jp

Abstract: The effects of plasma treatment of polyimide substrates on the texture and grain size distribution of aluminum thin films were studied. Oxygen-argon plasma treatment increased the average grain size and enhanced the (111) film texture. For short oxygen-argon plasma treatment times, the deposited Al films showed a (111) texture with a bimodal grain structure and even a {111}<11 $\bar{2}$ > type in-plane texture. The preferential nucleation and grain growth of (111) grains are discussed in terms of the interface energy anisotropy.

Keywords: aluminum thin film; polyimide; texture; plasma treatment

1. Introduction

Microstructure strongly influences the mechanical, electrical, and metallurgical properties of polycrystalline metal thin films. This correlation has received much attention in pure Al and Al alloys because of the importance of the reliability of these materials in microelectronics, where they are used as electrical conductors [1–10].

The microstructure of a thin film is influenced by the crystal structure of the substrate. When a crystalline film grows on a crystalline substrate and the lattices of the two match, the total periodic potential energy function is minimized so that the film grows epitaxially. For instance, Al can grow epitaxially on Si and rock salts [11], as well as on Ti {0001} surfaces [12,13]. For non-crystalline substrates, such periodic interaction hardly occurs. Instead, minimization of the film surface energy becomes a primary factor. The (111) texture of Al on thermally grown amorphous SiO₂ has been discussed with respect to surface energy minimization [14–16]. Minimization of the film-substrate interface energy is assumed to have the same effect as surface energy minimization, even though the interface energy could differ significantly from the surface energy. Most studies on grain growth in thin films on amorphous substrates have assumed that the interface energy is identical to the surface energy.

The interface energy is expected to influence the film texture as well as the film surface energy. It is well-known that contamination of the substrate reduces the grain size [17] and that gaseous impurities such as oxygen [15,18,19], nitrogen [18], and water vapor [18,19] reduce the grain size and change the texture. Thus, the chemical conditions of the substrate surface affect the grain growth during deposition and hence the microstructure.

The aim of the present study is to elucidate the influence of the surface chemical conditions of polyimide on the microstructure of Al films. The surface conditions were controlled by plasma pretreatment prior to Al deposition. Texture and grain growth are discussed in terms of the surface/interface energy minimization.

2. Experimental

PMDA-ODA (pyromellitic dianhydride oxydianiline, see Figure 1) polyimide type 2540 (DuPont™, Wilmington, DE, USA) was spun onto Si(100) wafers having a 100-Å-thick thermally grown oxide layer, baked in air at 250 °C for 30 min, and then cured in nitrogen at 400 °C for 60 min. The thickness of the polyimide films after the curing was about 200 nm.



Citation: Kondoh, E. Influence of Plasma Surface Treatment of Polyimide on the Microstructure of Aluminum Thin Films. *Coatings* **2022**, *12*, 334. <https://doi.org/10.3390/coatings12030334>

Academic Editor: Cheng Zhang

Received: 14 January 2022

Accepted: 28 February 2022

Published: 3 March 2022

Publisher's Note: MDPI stays neutral with regard to jurisdictional claims in published maps and institutional affiliations.



Copyright: © 2022 by the author. Licensee MDPI, Basel, Switzerland. This article is an open access article distributed under the terms and conditions of the Creative Commons Attribution (CC BY) license (<https://creativecommons.org/licenses/by/4.0/>).

Full conversion of the precursor to PMDA-ODA was confirmed by Fourier-transform infrared spectroscopy (Nicolet, Madison, WI, USA). An ultrahigh-vacuum direct-current magnetron sputtering apparatus (Angstrom Scientific, Ramsey, NJ, USA) with a base pressure of less than 2×10^{-6} Pa was used to deposit Al films. Prior to metallization, the substrate was dried in an oven at 150 °C for 30 min and then introduced immediately into the deposition chamber. For some experiments, 20- μm -thick PMDA-ODA polyimide (Kapton[®]) sheets were employed.

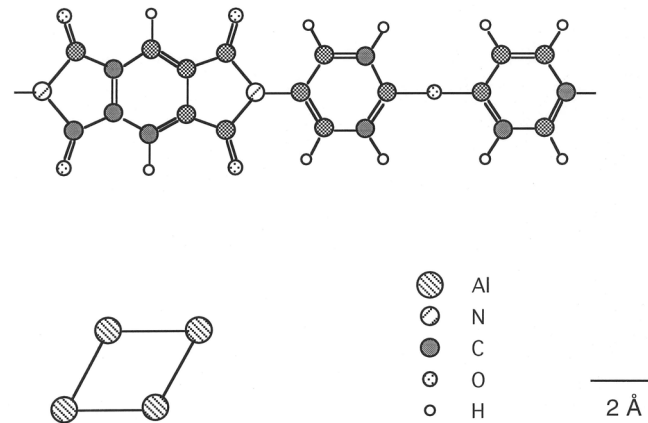


Figure 1. Structure of PMDA-ODA polyimide and Al (111) unit cell.

The metallization process involved an in situ cold plasma pre-treatment followed by Al deposition (see Figure 2). The in situ plasma pre-treatment was conducted using a radio-frequency plasma at a power density of about 0.3 W/cm^3 with a reactive ion etching arrangement, which forces a negative self-bias (ca. 850 V) upon the substrate and thus permits charged ion species to bombard the surface. The gas used was a mixture of $\text{O}_2/\text{Ar} = 1/15$ or pure (99.9999%) Ar. The plasma treatment times were 40 or 180 s. The gas flow rate was controlled by mass flow controllers. The total pressure was kept at 10 Pa.

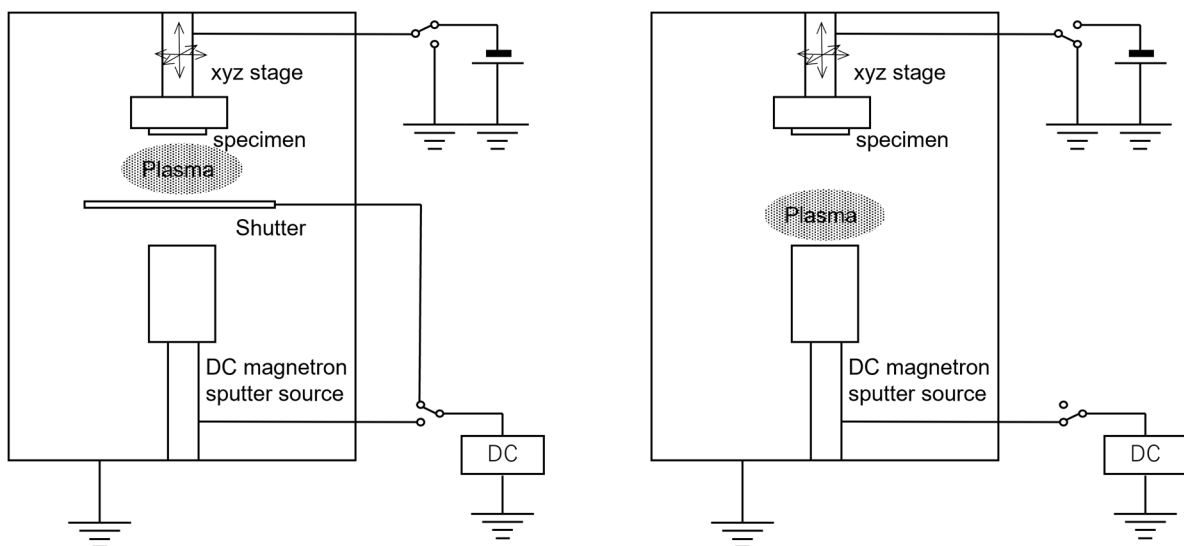


Figure 2. Experimental apparatus. Arrangement for plasma treatment (a) and for film deposition (b).

After evacuating the chamber down to the base pressure, a 1- μm -thick Al film was deposited from a pure (99.9999%) Al target in an Ar atmosphere at a pressure of about 0.7 Pa. The substrate pedestal was water-cooled during deposition. The microstructure of as-deposited Al films was characterized by transmission electron microscopy (TEM) and

the pole figure technique. For TEM observations and electron diffraction analyses, samples were cut into discs 3 mm in diameter, dimpled from the backside, and thinned by Ar ion-milling. The microscope (JEOL 2000FX, Tokyo, Japan) was operated at an acceleration voltage of 200 kV. The area of each individual grain, S , was measured, and the diameter of the equivalent circle was taken as the grain size, D , i.e., $D = (4S/\pi)^{1/2}$. To characterize the texture, a (111) pole figure was recorded in reflection geometry so as to obtain data at tilting angles between $\chi = 20^\circ$ (sample normal direction) and $\chi = 85^\circ$. Texture scans were performed using a 4-circle Siemens D5000 texture goniometer (Munich, Germany) with Cu $K\alpha$ radiation.

3. Results and Discussion

Figure 3a–d show TEM micrographs of Al films for different pretreatment conditions. The specimen pretreated by $O_2 + Ar$ plasma (hereafter, O_2 plasma) for 40 s (Figure 3b) exhibited grains that had grown to many times the size of the average grain. Selected-area diffraction (SAD) analysis revealed that most of these abnormal grains had (111) planes, while some grains had near {111} planes that tilted by as much as about 15° away from the film normal.

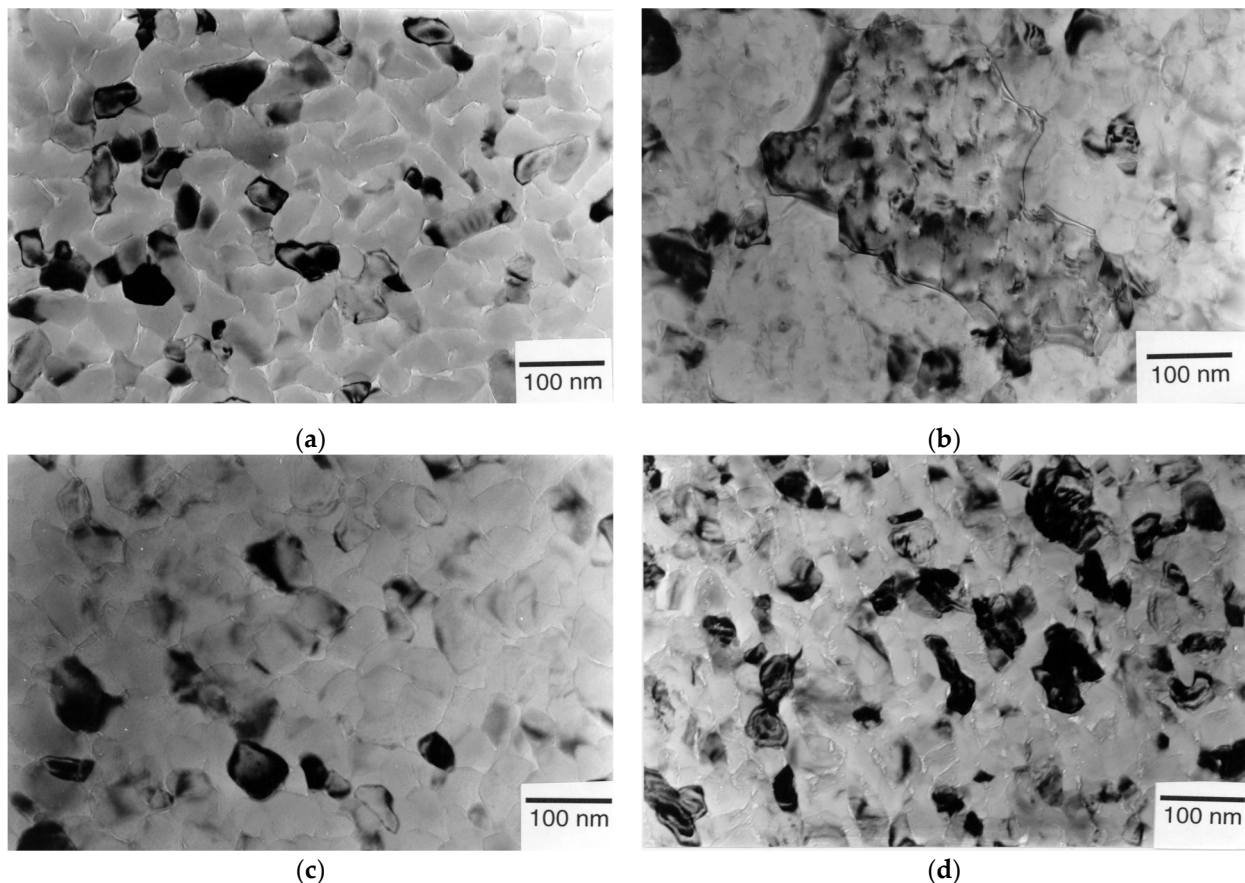


Figure 3. TEM micrographs of Al on polyimide. (a) Pristine; (b) O_2 plasma, 40 s; (c) O_2 plasma, 180 s; (d) Ar plasma, 180 s.

Figure 4 summarizes the intensities of the diffraction spots in the selected area diffraction (SAD) patterns. All the original diffraction patterns used in the analyses had ring patterns. Diffraction intensities are normalized against the 111 peak intensity. The concurrent appearance of intense 220 and 422 peaks indicates the presence of a (111) component parallel to the substrate. This can be seen in the large-selected-area (diameter: $100\ \mu\text{m}$) diffraction pattern for a Al film deposited on O_2 -plasma-treated polyimide (Figure 3b). The diffraction pattern from the normal grains of the bimodal structure (Figure 4) resembles that

from the random grains, except for slight strengthening of the 222 reflection. Subtraction of the spectrum of the normal grains from that of the total provides an intuitive understanding of the orientation of abnormal grains: the fact that only the 220 and 422 reflections remain significant suggests (111) texturing. The weakening of the 200 and 400 intensities can be seen for all the plasma-treated samples. This indicates the absence of a (100) component parallel to the substrate.

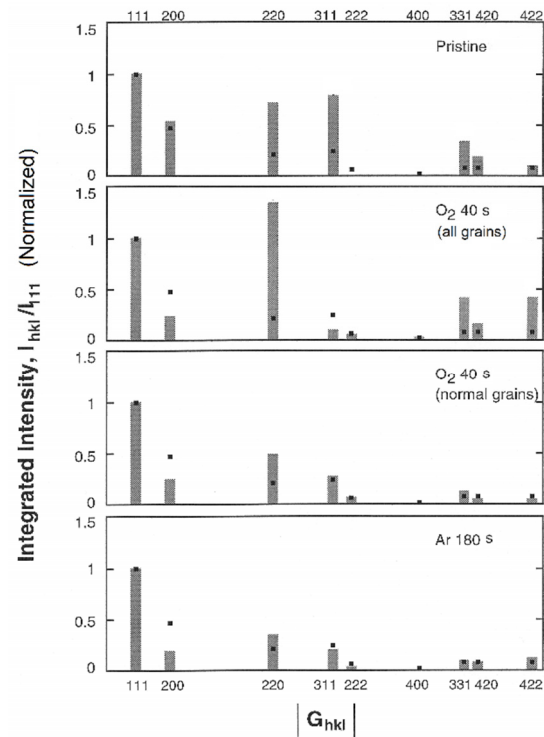


Figure 4. Summary of diffraction intensities obtained from selected-area TEM diffraction patterns of Al films. The intensities of random grains (JCPDS) were indicated by symbol ■.

Figure 5 shows (111) polar plots for the Al films. Plasma-treated samples show the most intense peaks at the center, which indicates the presence of a (111) fiber texture. The slight reduction in intensity at about 50° suggests the absence of a (100) component N_z , in accordance with the SAD patterns. The results of texture analyses by SAD and the polar figure technique are summarized in Table 1. The measured grain sizes are plotted on a log-normal probability chart (Figure 6). The probability function for the log-normal distribution, $\varphi(D)$, is given by

$$\varphi(D) = \frac{1}{\sigma D \sqrt{2\pi}} \exp\left[-\frac{(\ln D - \mu)^2}{2\sigma^2}\right], \quad (1)$$

where μ is the log-normal median and σ is the standard deviation. The Al film deposited after O_2 plasma treatment (40 s) had a clear bimodal distribution: two lines shifted away in parallel, showing an overlap of two different populations. Table 2 summarizes the grain size statistics. The O_2 -plasma-treated specimens had large mean grain sizes compared to the pristine or Ar-plasma-treated specimen. The bimodal distribution was deconvoluted into two log-normal components. Although the bimodal grains had a larger σ value of 0.24, the deconvoluted σ values did not differ significantly from the σ values for the other populations (normal grains).

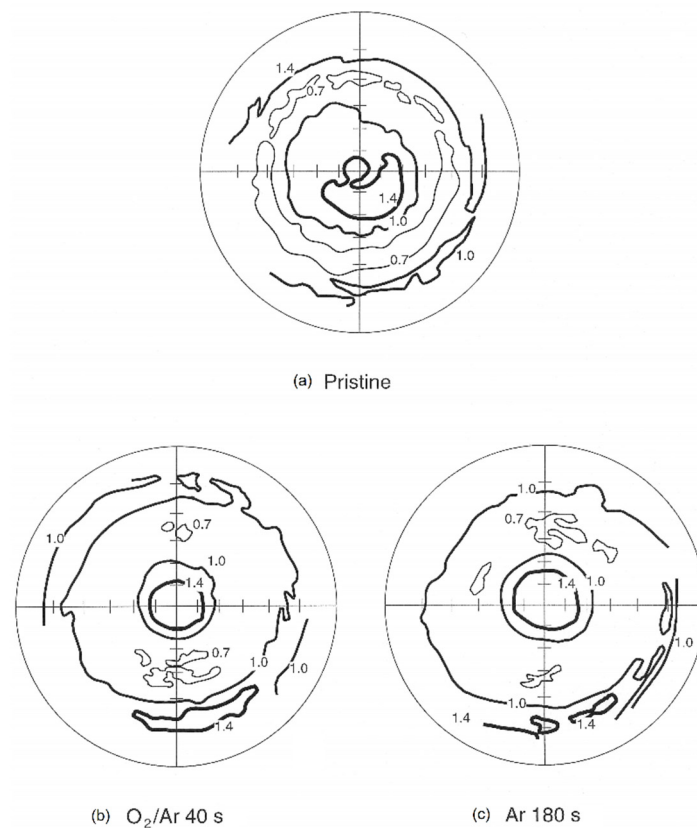


Figure 5. (111) polar plots obtained from Al films deposited on pristine (a), O₂/Ar plasma pretreated (b), and Ar plasma-treated polyimide (c).

Table 1. Summary of texture analyses.

Pretreatment	Texture	
None (pristine)	-	Unclear
O ₂ /Ar 40 s	Abnormal grains	(111) dominant
-	Normal grains	Random + (111)w – (100)w
Ar 180 s	-	Random + (111)w – (100)w

Table 2. Grain size statistics.

Pretreatment	Mean (nm)	Median (nm)	Standard Deviation (nm)
None (pretreatment)	66	62	0.16
O ₂ /Ar 40 s Total	168	140	0.24
Normal grains	-	121	0.18
Abnormal grains	-	494	0.11
O ₂ /Ar 180 s	93	83	0.16
Ar 180 s	68	64	0.15

Summarizing the experimental results described so far, the main effects of plasma pretreatment were (111) texturing and a change in the grain size distribution. Before discussing the origins of the film microstructure, let us give an overview of the chemical aspects of plasma pretreatment of the polyimide surface.

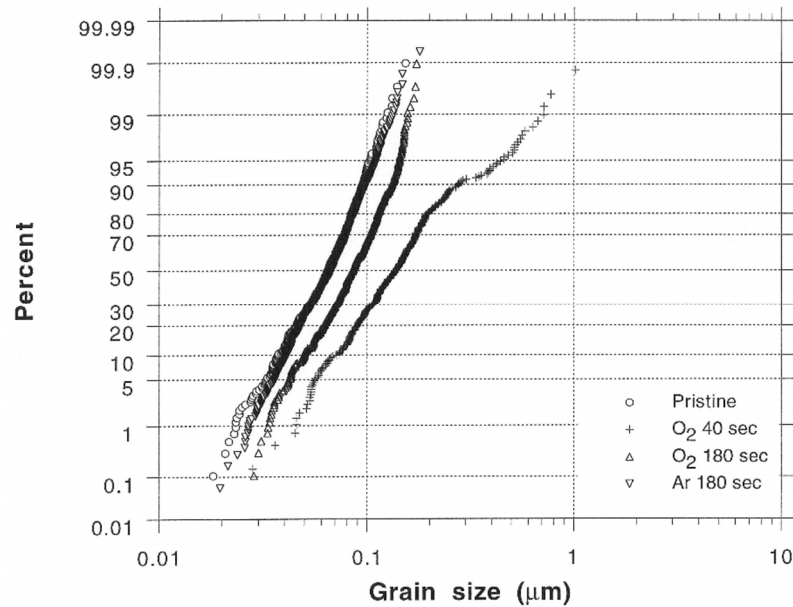


Figure 6. Log-normal plots of grain size distribution.

The reaction processes induced by plasma treatment of polyimide are understood as a sequence of polymer radical formation and the addition of simple radicals. Chain scission is a typical reaction that occurs on polyimide, forming polymer radicals [20–24]. Functional groups are then introduced by the addition of simple radicals to the polymer radicals. Oxygen plasma treatment of polyimide is known to significantly increase oxygen-containing functional groups such as carboxyl (COO) [23,25], carbonyl (=CO) [23], ethyl (>CO) [23], and hydroxyl (OH) groups [25]. Plasma treatment or ion bombardment using inert gases (e.g., He, Ar) also forms functional groups on polyimide [21,23]. X-ray photoelectron spectroscopy (XPS) [26–30] and high-resolution electron energy loss spectroscopy (HREELS) [31] have shown that evaporated Al reacts preferentially with the CO groups on the pristine polyimide surface and forms C–O–Al complexes. Other functional groups act as preferential adsorption sites for Al because of their high reactivity. Thus, the surface energy of polyimide increases with increasing concentration of added functional groups [22,32].

Next, we discuss the possible origins of the (111) texture and the grain size distribution, in particular the bimodal distribution, in view of the preferential nucleation of (111) grains and the grain growth during deposition. According to basic nucleation theory, the nucleation rate during Volmer–Weber type growth is expressed as [33]:

$$\dot{N} = N_0 \exp\left(-\frac{\Delta G_{\text{diff}} + \Delta G^*}{kT}\right), \quad (2)$$

where \dot{N} is the nucleation rate, N_0 is a pre-exponential factor, k is the Boltzmann constant, T is the absolute temperature, ΔG_{diff} is the activation energy for surface diffusion of metal atoms, and ΔG^* is the barrier energy for nucleation. Assuming isotropic surface energy and equilibrium conditions, the nuclei form a spherical cap whose contact angle is given by Young's balance:

$$\gamma_S = \gamma_{SC} + \gamma_C \cos \theta, \quad (3)$$

where γ_C is the surface energy of the nucleus, γ_S is the surface energy of the substrate, γ_{SC} is the nucleus-substrate interface energy, and θ is the contact angle. A smaller contact angle gives a lower ΔG^* and thus a higher \dot{N} . That is, a larger γ_S or smaller γ_{SC} or γ_C results in a higher nucleation rate. By taking into account the chemical bond energy per unit area of the interface, we reduce

$$\Delta\gamma_{SC} = \gamma_{SC}^* - \gamma_{SC}, \quad (4)$$

The appearance of particular Al planes on plasma-treated surfaces suggests energetic anisotropy in $\Delta\gamma_{SC}$, and thus $\Delta\gamma_{SC}$ can be described as a function of the orientation of a nucleus. Either γ_{SC}^* or γ_{SC} can be anisotropic.

One reason for the anisotropy in $\Delta\gamma_{SC}$ is epitaxy. Epitaxial growth would take place if the polyimide is crystalline or at least has a certain long-range arrangement of polymer chains. Aromatic units of polyimide have been reported to be stable against plasma treatment and not to be decomposed by a low ion dose [22,34]. Instead, as discussed above, plasma treatment introduces functional groups at particular sites in the aromatic rings. Thus, the functional groups would have three-fold symmetry. The three-fold symmetry of the Al (111) plane permits nuclei to grow in an epitaxial manner. One possible experimental evidence of epitaxial growth of Al on polyimide is shown in Figure 7. These (111) polar plots were obtained from 2- μm -thick Al films deposited on commercially available PMDA-ODA polyimide (Kapton[®]) sheets (20 μm) after O₂ plasma pretreatment for 40 s. The most striking feature is the three-fold symmetric peaks of (111) planes at around $\chi = 70^\circ$, accompanying faint (220) signals. The geometry of the (111) symmetry suggests the $\{111\}\langle 11\bar{2}\rangle$ in-plane alignment of (111) fiber grains. This type of in-plane texturing is commonly observed in epitaxially grown thin films on crystalline inorganic substrates but has not been reported for polymer substrates, to the best of the author's knowledge. The in-plane texturing was enhanced by post-deposition annealing. These results suggest the presence of a certain periodical ordering of the polyimide molecules. Unfortunately, there is very little consensus on the presence of long-range crystalline structure in polyimide [35,36]. Note that the in-plane stress in polyimide could be the cause of the anisotropy of the in-plane polymer arrangement. Longer plasma treatment (180 s) did not produce the in-plane texture and decreased the (111) peak intensity. This behavior can be correlated with the decrease in the (111) peak intensity observed for Al films spun on polyimide substrates.

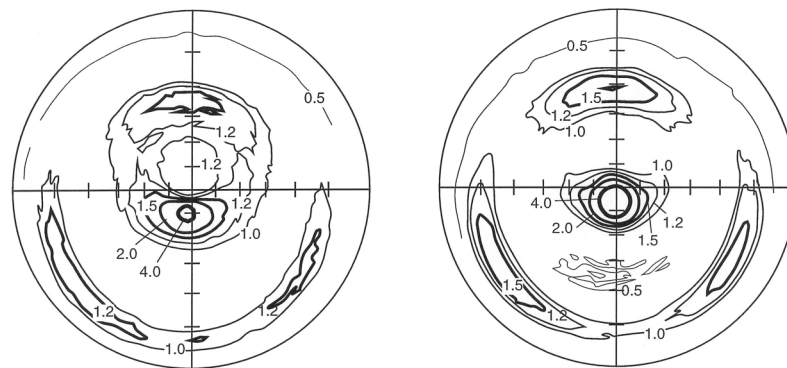


Figure 7. (111) polar plots obtained from 2- μm -thick Al films deposited on polyimide sheet after O₂ plasma pretreatment for 40 s. Before annealing (left) and after annealing (right) at 350 °C for 30 min.

If the reactivity of chemical species at the Al surface is dependent on the crystallographic plane of Al, this can be another mechanism for the anisotropy of $\Delta\gamma_{SC}$. The reactivity of oxygen on Al surfaces decreases in the order (111) > (110) > (100) [37]. (111) planes are most likely to react with the oxygen-containing groups at treated polyimide rings, resulting in preferential nucleation of (111) planes. This model seems more advantageous than the epitaxy model discussed above, since it does not require the presence of a periodic structure in polyimide. However, it cannot explain the in-plane texturing simply.

The Al film deposited after 40 s of O₂ plasma pretreatment had a larger average grain size and contained abnormal grains. The presence of abnormal grains indicates that grain growth occurred during film thickening [16]. When the orientations of two adjacent grains are different, the difference in surface energy produces an additional driving force that overcomes grain boundary pinning [38]. A difference in surface energy of only a few percent is large enough to mobilize grain boundaries. Thus, in the case of Al, most abnormal grains have lower energy planes like (111) and the film has a (111) texture.

It is noteworthy that grains with a weak (111) texture did not contain abnormal grains, as seen in the case of Ar plasma pretreatment (Figure 4). This suggests that abnormal grain growth does not start unless the amount of preferential grains is above a certain threshold. Similarly, the primary grains (normal grains) of a bimodal structure (O₂, 40 s) are weakly (111) textured. This implies that not all low-energy grains grow abnormally. A simulation study by Frost, Thompson, and Walton [39] has shown that abnormal grain growth does not occur in a matrix that consists of randomly orientated grains, even if sufficient surface energy anisotropy is present. “Seeding” of a significant fraction of low-energy grains was needed to initiate abnormal grain growth; only some of the seeded grains grew abnormally. It has also been shown that the fraction of seeded grains is dependent on the level of additional driving forces for grain boundary migration. These simulation results support our experimental data: the “seeding” induced by the preferential nucleation of (111) planes leads to (111) texturing and a bimodal distribution. Although the critical fraction of seeded grains has not been established quantitatively, our rough estimate on the basis of SAD analyses is a few percent.

4. Conclusions

Plasma pretreatment of the polyimide surface introduces O-containing functional groups and increases the number of sites where Al atoms can be adsorbed. The interaction between the functional groups and Al plays a primary role in the nucleation of Al grains. The (111) texture of Al films deposited on plasma-pretreated substrates stems from the anisotropy of the Al-polyimide interface energy. Epitaxial growth would occur if the polyimide structure has a long-range order and if the adsorption sites have high symmetry. The crystallographic plane dependence of the chemical reactivity of the Al surface is discussed as another possibility. The former type of anisotropy is attributable to polyimide itself, while the latter is due to Al. Judging from the three-fold (111)<11 $\bar{5}$ > in-plane texture of the Al films, we concluded that the epitaxial growth argument is more plausible. The (111) texture develops through grain growth during deposition, driven by the preferential nucleation of (111) planes. Selective area diffraction analysis suggests that the fraction of (111) grains needs to be above a threshold (of a few percent) for the development of an abnormal grain structure. The microstructure analyses of this study provide the basis for understanding electrical and or mechanical properties of metal/polymer film stacks.

Funding: This work was in part supported by JSPS KAKENHI Grant Nos. JP19K04466 and JP20K04518.

Institutional Review Board Statement: Not applicable.

Informed Consent Statement: Not applicable.

Data Availability Statement: Data sharing is not applicable to this article.

Conflicts of Interest: The authors declare no conflict of interest.

References

1. Attardo, M.J.; Rutledge, R.; Jack, R.C. Statistical Metallurgical Model for Electromigration Failure in Aluminum Thin-Film Conductors. *J. Appl. Phys.* **1971**, *42*, 4343–4349. [[CrossRef](#)]
2. Schoen, J.M. Monte Carlo calculations of structure-induced electromigration failure. *J. Appl. Phys.* **1980**, *51*, 513–521. [[CrossRef](#)]
3. Cho, J.; Thompson, C.V. Grain size dependence of electromigration-induced failures in narrow interconnects. *Appl. Phys. Lett.* **1989**, *54*, 2577–2579. [[CrossRef](#)]
4. Vaidya, S.; Sheng, T.T.; Sinha, A.K. Linewidth dependence of electromigration in evaporated Al-0.5%Cu. *Appl. Phys. Lett.* **1980**, *36*, 464–466. [[CrossRef](#)]
5. Vaidya, S.; Sinha, A.K. Effect of texture and grain structure on electromigration in Al-0.5%Cu thin films. *Thin Solid Film.* **1981**, *75*, 253–259. [[CrossRef](#)]
6. Knorr, D.B.; Rodbell, K.P. The role of texture in the electromigration behavior of pure aluminum lines. *J. Appl. Phys.* **1996**, *79*, 2409–2417. [[CrossRef](#)]
7. Liu, X.; Li, Y.; Liu, Y.; Sun, D.; Guo, W.; Sun, X.; Feng, Y.; Chi, H.; Li, X.; Tian, F.; et al. Performance and microstructure characteristics in polyimide/nano-aluminum composites. *Surf. Coat. Technol.* **2017**, *320*, 103–108. [[CrossRef](#)]

8. Lucchini, R.; Cattarinuzzi, E.; Maraghechi, S.; Gastaldi, D.; Adami, A.; Lorenzelli, L.; Vena, P. Delamination phenomena in aluminum/polyimide deformable interconnects: In-situ micro-tensile testing. *Mater. Des.* **2016**, *89*, 121–128. [[CrossRef](#)]
9. Liu, D.S.; Tsai, C.Y.; Lu, Y.T.; Sung, C.K.; Chung, C.L. Finite element method investigation into nanoimprinting of aluminum/polyimide bi-layer substrates. *Mircoelectr. Eng.* **2010**, *87*, 2361–2367. [[CrossRef](#)]
10. d’Heurle, F.; Berenbaum, L.; Rosenberg, R. On the structure of aluminum films. *Trans. Metall. Soc. AIME* **1968**, *242*, 502–511.
11. Jawarani, D.; Stark, J.P.; Kawasaki, H.; Olowolafe, J.O.; Lee, C.C.; Klein, J.; Pintchovski, F. Intermetallic Compound Formation in Ti/Al Alloy Thin Film Couples and Its Role in Electromigration Lifetime. *J. Electrochem. Soc.* **1994**, *141*, 302–305. [[CrossRef](#)]
12. Knorr, D.B.; Szpunar, J.A. Applications of texture in thin films. *J. Met.* **1994**, *46*, 42–48. [[CrossRef](#)]
13. Sinha, A.K.; Sheng, T.T. The temperature dependence of stresses in aluminum films on oxidized silicon substrates. *Thin Solid Film.* **1978**, *48*, 117–126. [[CrossRef](#)]
14. Roberts, S.; Dobson, P.J. The microstructure of aluminium thin films on amorphous SiO₂. *Thin Solid Film.* **1986**, *135*, 137–148. [[CrossRef](#)]
15. Knorr, D.B.; Tracy, D.P.; Lu, T.-M. Texture development in thin metallic films. *Textures Microstruct.* **1991**, *14*, 543–554. [[CrossRef](#)]
16. Grovenor, C.R.M.; Hentzell, H.T.G.; Smith, D.A. The development of grain structure during growth of metallic films. *Acta Metall.* **1984**, *32*, 773–781. [[CrossRef](#)]
17. Silvain, J.F.; Veyrat, A.; Ehrhardt, J.J. Influence of oxygen partial pressure on the adhesion of metallic films evaporated on PET. *Thin Solid Film.* **1994**, *237*, 164–171. [[CrossRef](#)]
18. Verkerk, M.J.; Van der Kolk, G.J. Effects of oxygen on the growth of vapor-deposited aluminum films. *J. Vac. Sci. Technol. A* **1986**, *4*, 3101–3105. [[CrossRef](#)]
19. Ferl, J.E.; Edward, J.; Long, R. Infrared spectroscopic analysis of the effects of simulated space radiation on a polyimide. *IEEE Trans. Nucl. Sci.* **1981**, *28*, 4119–4124. [[CrossRef](#)]
20. Matienzo, L.J.; Emmi, F.; Hart, D.C.V.; Gall, T.P. Interactions of high-energy ion beams with polyimide films. *J. Vac. Sci. Technol. A* **1989**, *7*, 1784–1789. [[CrossRef](#)]
21. Egitto, F.D.; Matienzo, L.J.; Blackwell, K.J.; Knoll, A.R. Oxygen plasma modification of polyimide webs: Effect of ion bombardment on metal adhesion. *J. Adhes. Sci. Technol.* **1994**, *8*, 411–433. [[CrossRef](#)]
22. Inagaki, N.; Tasaka, S.; Hibi, K. Improved adhesion between plasma-treated polyimide film and evaporated copper. *J. Adhes. Sci. Technol.* **1994**, *8*, 395–410. [[CrossRef](#)]
23. Fatyeyeva, K.; Dahi, A.; Chappey, C.; Langevin, D.; Valleton, J.-M.; Poncin-Epaillard, F.; Marais, S. Effect of cold plasma treatment on surface properties and gas permeability of polyimide films. *RSC Adv.* **2014**, *4*, 31036–31046. [[CrossRef](#)]
24. Tanigawa, S.; Nakamae, K.; Matsumoto, T. Effect of the radio frequency O₂ plasma treatment at polyimide surface on the adhesion of the vacuum deposited thin Fe Film. *Kobunshi Ronbunshu* **1990**, *47*, 41–48. [[CrossRef](#)]
25. Altanasoska, L.; Anderson, S.G.; Meyer, H.M., III; Lin, Y.; Weaver, J.H. Aluminum/polyimide interface formation: An x-ray photoelectron spectroscopy study of selective chemical bonding. *J. Vac. Sci. Technol. A* **1987**, *5*, 3325–3333. [[CrossRef](#)]
26. Bartha, J.W.; Hahn, P.O.; LeGoues, F.; Ho, P.S. Photoemission spectroscopy study of aluminum–polyimide interface. *J. Vac. Sci. Technol. A* **1995**, *3*, 1390–1393. [[CrossRef](#)]
27. Pireaux, J.J. Is there an interaction at the aromatic site(s) in a metal/polymer interface? An XPS and HREELS review. *Synth. Met.* **1994**, *67*, 39–46. [[CrossRef](#)]
28. Park, S.J.; Lee, E.J.; Kwon, S.H. Influence of atmospheric-pressure plasma treatment on surface of polyimide film. *Solid State Phenom.* **2007**, *119*, 123–126. [[CrossRef](#)]
29. Usami, K.; Ishijima, T.; Toyoda, H. Rapid plasma treatment of polyimide for improved adhesive and durable copper film deposition. *Thin Solid Film.* **2012**, *521*, 22–26. [[CrossRef](#)]
30. Ho, P.S.; Hahn, P.O.; Bartha, J.W.; Rubloff, G.W.; LeGoues, P.K.; Silverman, B.D. Chemical bonding and reaction at metal/polymer interfaces. *J. Vac. Sci. Technol. A* **1985**, *3*, 739–745. [[CrossRef](#)]
31. Cen-Puc, M.; Schander, A.; Vargas Gleason, M.G.; Lang, W. An Assessment of Surface Treatments for Adhesion of Polyimide Thin Films. *Polymers* **2021**, *13*, 1955. [[CrossRef](#)] [[PubMed](#)]
32. Kenty, J.L.; Hirth, J.P. Epitaxy and heterogeneous nucleation theory. *Surf. Sci.* **1969**, *15*, 403–424. [[CrossRef](#)]
33. Baglin, J. Ion beam modification of insulators. *Surf. Sci. Lett.* **1987**, *191*, A524.
34. Bachman, B.J.; Vasile, M.L. Ion bombardment of polyimide films. *J. Vac. Sci. Technol. A* **1980**, *7*, 2709–2716. [[CrossRef](#)]
35. Oberlin, A.; Ayache, J.; Oberlin, M. High-resolution dark-field imaging in epoxy and polyimide systems. *J. Polym. Sci. Polym. Phys. Ed.* **1982**, *20*, 579–591. [[CrossRef](#)]
36. Russel, T.R. A small-angle X-ray scattering study of an aromatic polyimide. *J. Polym. Sci. Polym. Phys. Ed.* **1984**, *22*, 1105–1117. [[CrossRef](#)]
37. Iona, F. Preparation and properties of clean surfaces of aluminum. *J. Phys. Chem. Solids* **1967**, *28*, 2155–2158.
38. Mullins, W.W. The effect of thermal grooving on grain boundary motion. *Acta Metall.* **1958**, *6*, 414–427. [[CrossRef](#)]
39. Frost, H.J.; Thompson, C.V.; Walton, D.T. Simulation of thin film grain structures—II. Abnormal grain growth. *Acta Metall. Mater.* **1992**, *40*, 779–793. [[CrossRef](#)]